Regulate the content of BCC and Sigma phases to achieve precise control of the performance of AlxCoCr_{0.6}NiV_{0.6} high entropy alloy through heat treatment

Wu Da, Li Bo*, Tian Mengyao, Shi Yuzhi, Gao Yimin, Li Cong*, Wu Tao, and Pan Tingjiang

State Key Laboratory for Mechanical Behaviour of Materials, School of Materials Science and Engineering, Xi'an Jiaotong University, Xi'an 710049, China

*Corresponding address: e-mail: libo616@mail.xjtu.edu.cn

Abstract: In this study, the effect of heat treatment on the microstructure and mechanical properties of Al_{0.4}CoCr_{0.6}NiV_{0.6} high entropy alloy were investigated. Regulating the heat treatment temperature enabled precise control over the contents and distributions of the FCC matrix, BCC phase, and Sigma phase in the alloy. This led to the optimization of its microstructure and mechanical properties. Research revealed that within the heat treatment temperature range of 1000°C-1150°C, the Sigma phase in the samples predominantly existed as particles within the BCC phase interface. Upon elevating the heat treatment temperature to 1200°C, the Sigma phase tended to align along the BCC phase boundaries. The volume fraction of the brittle Sigma phase rosed firstly and then declined with the increase of heat treatment temperature, reaching a maximum at 1050°C. In order to analyse the effect of heat treatment on the mechanical properties of the alloy, room temperature compression and microhardness were performed. Results indicated that the compressive yield strength of the specimens initially rosed and then felled with increasing heat treatment temperature. Specifically, the compressive yield strength of the alloy after 1050°C heat treatment attained 1080 MPa and had increased by 92.8 % compared with the as-cast alloy of 560 MPa, which was primarily attributed to the second phase strengthening effect induced by the brittle Sigma phase. Overall, both the compressive yield strength and microhardness of the heat treated alloys were higher than that of the as-cast alloy.

Keywords: High entropy alloy; Heat treatment; Sigma phase; Microstructure; Mechanical property

1 Introduction

High-entropy alloys (HEAs), characterized by their vast compositional design and structural tunability, have garnered significant attention since their inception [1, 2]. Among them, CoCrNi-based HEAs have received particular attention due to their excellent ductility and plasticity [3-5]. However, the relatively low yield strength of as-cast CoCrNi alloys (<400 MPa) limits their engineering applications under extreme conditions [6].

Currently, various studies have been conducted to strengthen CoCrNi-based HEAs: (1) alloying induce lattice distortion and solid-solution strengthening, significantly enhancing alloy strength [7-9]; (2) innovative fabrication processes, such as selective laser melting and spark plasma sintering, which eliminate casting defects and improve the properties of CoCrNi-based HEAs [10, 11]; (3) strain hardening induced by plastic deformation to strengthen CoCrNi-based HEAs [12-14]; (4) microstructural optimization through heat treatment enhance the

mechanical properties of CoCrNi-based HEAs [15]; and (5) second-phase precipitation strengthening through in situ synthesis of secondary phase particles [16, 17]. Although many methods for strengthening CoCrNi-based HEAs have been developed, most studies still focused on alloying strengthening. Among them, the initial research direction was to add a single alloying element for strengthening. Lu et al. [18] introduced Nb into the CoCrNi alloy, which led to the precipitation of the hardening phase y'. This modification significantly enhanced the ductility and high-strength strain-hardening capability of the CoCrNiNb alloy. Niu et al. [19] discovered that the addition of Al induced significant lattice distortion in the alloy, which facilitated phase transitions and subsequently increased the alloy's ultimate tensile strength (UTS) to 899 MPa. To further enhance the performance of alloy. Zhang et al. [20] added Al and Nb to CoCrNi-based HEA. This significantly increased the UTS of the CoCrNiNbAl alloy to 1027 MPa but reduced the fracture strain was

reduced to 12.5%. The effectiveness of two-element alloying strengthening method was confirmed in our prior work. Shi et al. ^[21] investigated that volume fraction of σ phase can be controlled by adjusting the Al content in CoCrNiVAl HEA. Wu et al. ^[22] found that the compressive yield strength of Al_xCoCr_{0.6}NiV_{0.6} HEA showed a trend of increasing first and then decreasing with the increase of Al content. The compressive yield strength of the Al_{0.4}CoCr_{0.6}NiV_{0.6} HEA was 570 MPa, and the alloy didn't break. However, the yield strength of Al_{0.6}CoCr_{0.6}NiV_{0.6} HEA rised to 2.0 GPa with the increase of Al content. Correspondingly, the fracture strain of the alloy dropped to 15%. Evidently, high strength without overly sacrificing the plasticity of the alloy remained an important challenge.

Strategies such as heat treatment to regulate the content of different phases in alloys have been used to further improve the mechanical properties of alloys [23-27]. Uporov et al. [23] reported that due to the precipitation of Sigma phase, the AlCoCrFeNiMn HEA has better mechanical properties after heat treatment at 1400K. Huang et al. [24] adjusted the morphology of the L1₂ phase in Ni₃₅Co_{27.5}Cr_{27.5}Al₅Ti₅ HEA through heat treatment, enabling the UTS of the alloy to reach 1220 MPa. Ji et al. significantly improved the high-temperature mechanical properties of the alloy by regulating the γ 'phase in (CoCrNi)94(TiAl)6 HEA through heat treatment. Peng et al. [26] reported that the properties of alloy can be improved by regulating the volume fraction of the L12 phase in (CoCrNi)94Ti3Al3 HEA through heat treatment. In summary, it was an effective method in the mechanical properties of alloys by adjusting the precipitate content through heat treatment.

Based on the previous work of our research, Al_{0.4}CoCr_{0.6}NiV_{0.6} HEA was selected as the research object in this study. The effects of different heat treatment temperatures on the microstructure and mechanical properties of Al_{0.4}CoCr_{0.6}NiV_{0.6} HEA were investigated. The compressive yield strength and microhardness of the Al_{0.4}CoCr_{0.6}NiV_{0.6} HEA were tested in detail at room temperature. The relationship between heat treatment temperature and microstructure was established through EBSD and TEM characterization, and the intrinsic relationship between microstructure and mechanical properties was revealed.

2 Experimental section

Al_{0.4}CoCr_{0.6}NiV_{0.6} HEA was prepared by vacuum arc melting using Co, Cr, Ni, V, and Al metal particles with purities exceeding 99.9% as raw materials. The melting process involved the following steps: The vacuum arc melting furnace (MSM20-7, Shenyang Kejing Automation Equipment Co., LTD.) was continuously evacuated for 3 minutes, followed by the continuous injection of argon gas for 1 minute. This cycle was repeated three times. In the final cycle, argon gas was introduced to achieve a chamber pressure of -0.05 MPa. The current was 160 A during the melting process. To ensure compositional homogeneity, each sample was subjected to six remelting cycles, resulting in a button-shaped ingot with a diameter of approximately 30 mm and a thickness of approximately 10 mm. The specific component of the alloy was shown in Table 1.

Table 1. Composition of Al_{0.4}CoCr_{0.6}NiV_{0.6} alloy (at.%)

Al	Со	Cr	Ni	V
0.1529	0.2647	0.1588	0.2647	0.1588

The prepared button samples were then subjected to vacuum heat treatment in an atmosphere tube furnace (GSL-1600X, Hefei Kejing Material Technology Co., LTD.). The heat treatment temperatures were 1000°C, 1050°C, 1100°C, 1150°C, and 1200°C, respectively. The naming and heat treatment process of alloy were shown in Table 2. The specific process was depicted in Fig. 1. The samples were heated to the respective temperatures at a rate of 10°C/min, held for 10 hours, and then cooled to room temperature with the furnace. After heat treatment, the samples were wire-cut to the required dimensions and subsequently ground with #400, #800, #1200, #1500, and #2000 sandpaper. Finally, the samples were polished using a diamond suspension.

Table 2. Heat treatment process of the alloy

Sample	Temperature (°C)	Time (h)
As cast	-	-
HT 1000	1000	10
HT 1050	1050	10
HT 1100	1100	10
HT 1150	1150	10
HT 1200	1200	10

Samples with dimensions of $10\text{mm} \times 5\text{mm} \times 1\text{mm}$ were used for X-ray diffraction (XRD) analysis. The XRD measurements were performed using Cu-K α

radiation at 40 kV and 40 mA, with a scanning angle ranging from 20° to 90°. The microstructure of the alloy was observed using a scanning electron microscope (SEM) (FEI QUANTA 650 FEG). Electron backscatter diffraction (EBSD) image data were collected using the scanning electron microscope and analyzed with AZtCrystal software. High-resolution images of the samples were obtained using a Talos F200X transmission electron microscope (TEM), and the collected TEM data were analyzed using Digital Micrograph software.

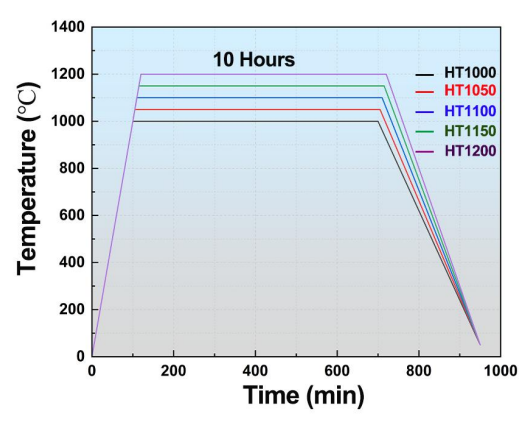


Fig. 1: Technology for heating processing

The microhardness of the alloy was measured using an HXD-type 1000 Vickers hardness tester. The test parameters included a load of 200 g and a loading time of 15 s. To ensure the reliability of the results, six different locations along the diagonal were selected for microhardness measurement. Room-temperature compression experiments were conducted on a universal testing machine (CMT4503) using cylindrical specimens with dimensions of 4mm × 6mm. To ensure the accuracy of the compression data, every alloy tested at least three samples.

3 Results and discussion

3.1 Microstructure

Fig. 2 presents the XRD patterns of the alloy under different heat treatment conditions. The as-cast alloy exhibites diffraction peaks corresponding to the FCC and L1₂ phases, specifically at (111), (200), and (220). These peaks are indicative of the balanced multi-component nature of the alloy. In contrast, the XRD pattern of the alloy after heat treatment clearly reveal the presence of the Sigma phase. This finding suggests that the heat treatment promotes the precipitation of the Sigma phase.

To further investigate the effect of heat treatment temperature on the microstructure of Al_{0.4}CoCr_{0.6}NiV_{0.6}

HEA, the microstructure of the alloy after various heat treatment is analyzed using scanning electron microscopy (SEM) and the results present in Fig. 3. The as-cast alloy exhibits a uniform microstructure without any obvious precipitated phases (Fig. 3a). After heat treatment at 1000°C, the HT1000 alloy shows significant precipitation of body-centered cubic (BCC) and σ phases (Fig. 3b). When the heat treatment temperature is increased to 1050°C, the σ phase in the HT1050 alloy is distributed along the interior of the BCC phase (Fig. 3c). The content of BCC and σ phases in the alloy are significant reduced 1150°C after heat treatment (Fig. 3e). heat-treatment at 1200°C, the microstructure of the alloy contains FCC and BCC structures, with no evident σ phase precipitation (Fig. 3f).

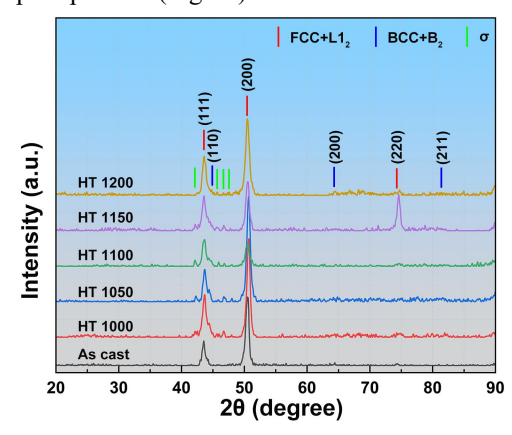


Fig. 2: XRD pattern of the alloy under different heat treatment conditions

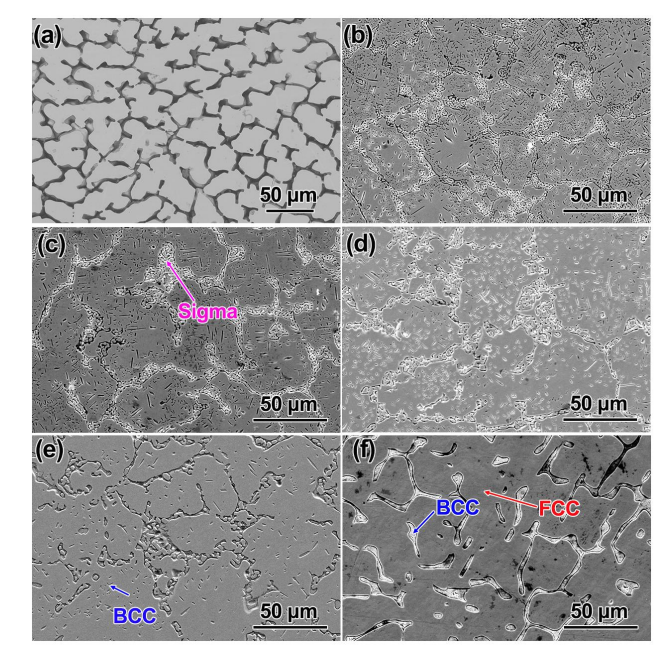


Fig. 3: SEM images of the alloy after heat treatment: (a) as-cast, (b) HT1000, (c) HT1050, (d) HT1100, (e) HT1150, (f) HT1200

To elucidate the phase distribution of the alloy after different heat treatment temperatures, electron backscatter diffraction (EBSD) analysis is conducted on each specimen in this study, with the results present in Fig. 4. Overall, the microstructures of all specimens are composed of face-centered cubic (FCC), body-centered cubic (BCC), and σ phases. As shown in Fig. 4(a), the HT1000 alloy exhibits BCC structures, which distributes throughout the FCC matrix. Meanwhile, the majority of the σ phase is primarily located within the BCC phase and partial σ phase precipitates in the FCC matrix. As the heat treatment temperature increased to 1050°C, the σ phase disappears in the FCC matrix, while a significant amount of σ phase is observed within the BCC phase structure

(Fig. 4b). Further elevation of the heat treatment temperature leads to a reduction in both the BCC and σ phase contents in the HT1100 specimen (Fig. 4c). When the temperature is further raised to 1150°C, compared with the HT1100 specimen, the BCC phase content in the HT1150 specimen remains essentially unchanged, but the σ phase content decreases significantly (Fig. 4d). Notably, at a heat treatment temperature of 1200°C, the HT1200 specimen contains minimal σ phase, which shifts from a granular distribution to one along the BCC phase boundaries. Concurrently, the acicular BCC structures in the FCC matrix disappears, and only a few vermiform BCC phase structures are observed within the FCC matrix (Fig. 4e).

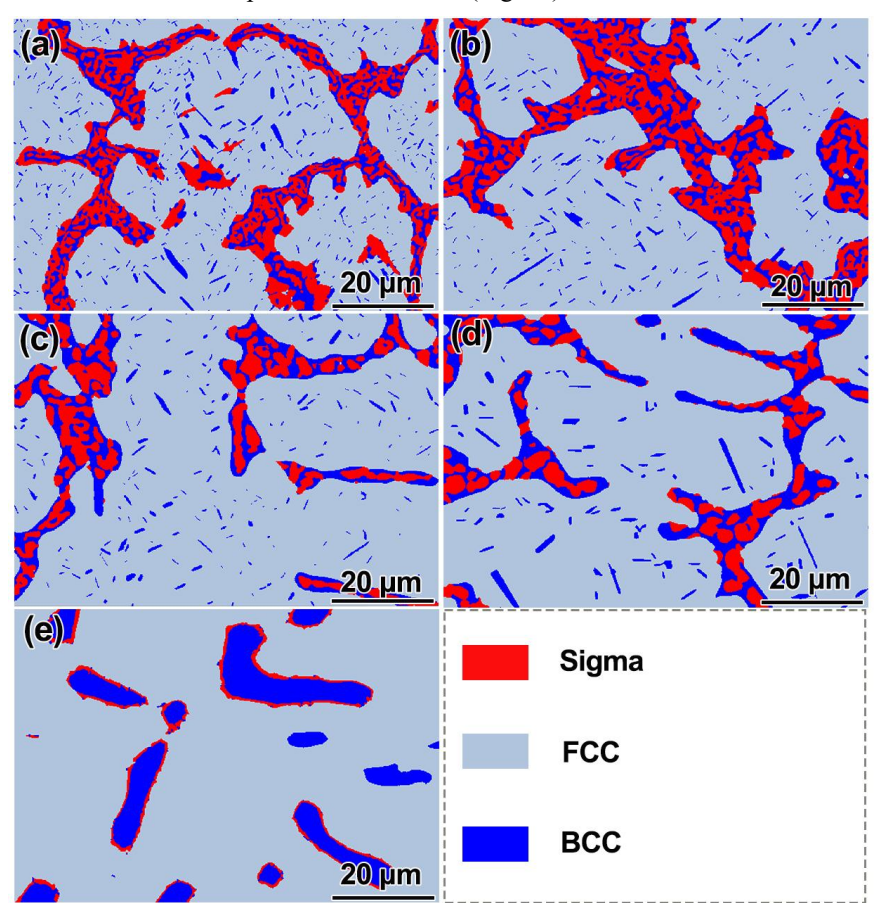


Fig. 4: Phase distribution of the alloy after heat treatment: (a) HT1000, (b) HT1050, (c) HT1100, (d) HT1150, (e) HT1200

The influence of heat treatment temperatures on the phase composition of the alloy is explored through statistical analysis based on the EBSD results. The analysis is conducted for the distribution of FCC, BCC and Sigma phase contents in each sample. The relevant data is shown in Table 3. Table 3 shows that when the heat treatment temperature rises, the content of the FCC phase first decreases and then increases, while the contents of the BCC and Sigma phases first increase and then decrease. Compared with the HT1000 sample, it is found that the FCC content of the HT1050 sample

decreases, the BCC content slightly increases, and the content of the hard and brittle Sigma phase increases to 19.6%. When the heat treatment temperature continues to rise, the FCC content gradually increases, while the contents of BCC and Sigma phases show a downward trend. It is particularly worth noting that the content of Sigma phase in the HT1200 sample is only 3.2%, which is approximately 83.7% lower than that in the HT1050 sample. It indicates that heat treatment has a significant influence on the phase composition of the alloy.

Table 3. Statistics of phase content of each sample under different heat treatment conditions

Sample	FCC/%	BCC/%	Sigma(σ)/%
HT 1000	70.1	12.9	17
HT 1050	66.8	13.6	19.6
HT 1100	78.9	12.9	10.2
HT 1150	79.5	12.6	7.9
HT 1200	84.7	12.1	3.2

Fig. 5 presents the Inverse Pole Figure (IPF) of each specimen under different heat treatment conditions. The coarse body-centered cubic (BCC) structure in the HT1000, HT1050, and HT1100 samples tend toward the (101) crystal orientation, while the face-centered cubic (FCC) phase does not exhibit a significant orientation relationship, as shown in Figs. 5(a), 5(b), and 5(c),

respectively. Notably, the fine needle-like BCC phase also lacks an obvious crystal orientation relationship. As the heat treatment temperature increases to 1150°C, the IPF pattern of the HT1150 sample reveals that a small portion of the BCC phase is distributed along the (111) crystal direction, with the corresponding FCC phase showing a similar distribution, as depicted in Fig. 5(d). When the heat treatment temperature is further elevated to 1200°C, almost all BCC phases in the HT1200 sample are completely shifted towards the (111) crystal direction, as illustrated in Fig. 5(e). It indicates that the increase in heat treatment temperature promotes the transformation of the BCC phase's crystal orientation, specifically a gradual shift from the (101) to the (111) orientation. Additionally, the σ phase in all samples don't display an obvious crystal orientation relationship.

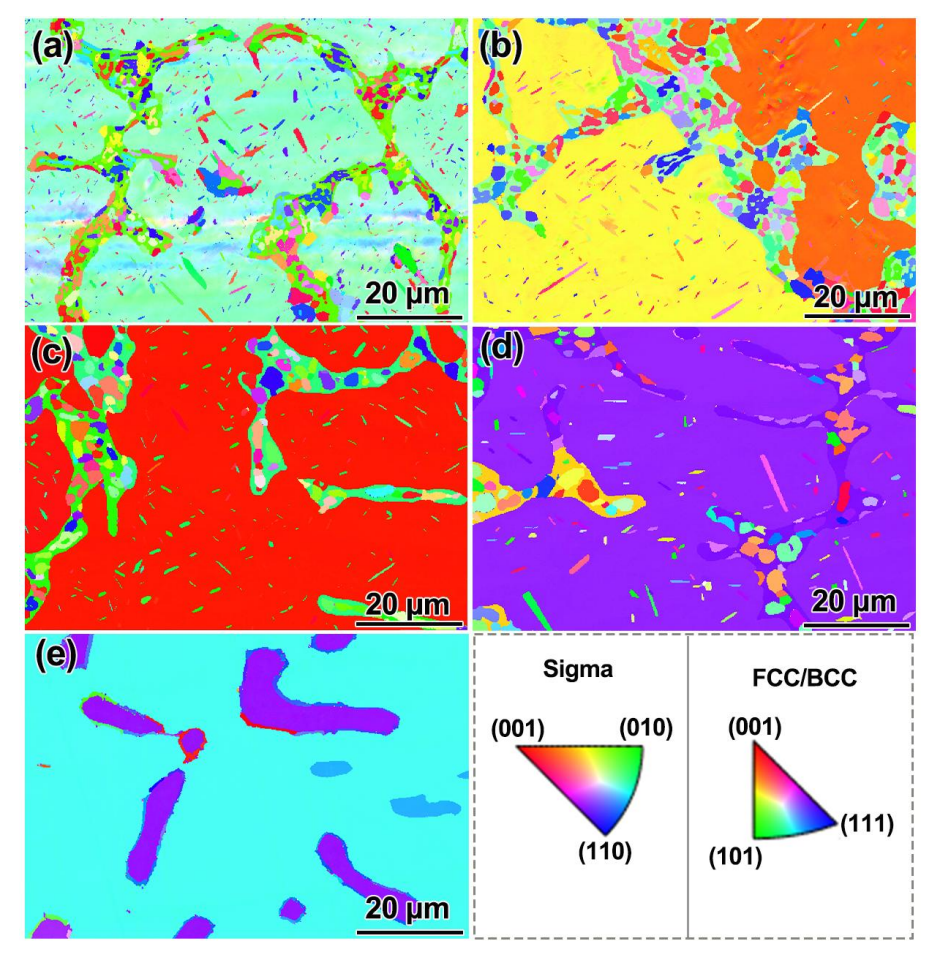


Fig. 5: IPF of alloy after heat treatment: (a) HT1000, (b) HT1050, (c) HT1100, (d) HT1150, (e) HT1200

TEM analysis of HT1050 alloy is presented in Fig. 6. Panel i of Fig. 6(a) displays the high-resolution image of HT1050 alloy. The Fourier transform of this image (inset in panel i of Fig. 6a) confirms a BCC crystal structure. The inverse fractional Fourier transform (IFFT) reveals the BCC phase (panel i of Fig. 6b), with a measured interplanar spacing of 0.2157 nm. Stress distribution

analysis in the BCC structure (Panel i of Fig. 6c) shows uneven tensile and compressive stress distributions, with tensile stress dominating, indicating significant sample tensile stress. Panel ii of Fig. 6(a) shows the Sigma phase's TEM image in sample HT1050. The IFFT (panel ii of Fig. 6b) indicates the Sigma phase with an interplanar spacing of 0.313 nm. Stress analysis in the

Sigma phase (panel ii of Fig. 6c) reveals a more uniform stress distribution, with compressive and tensile stresses

being approximately equal.

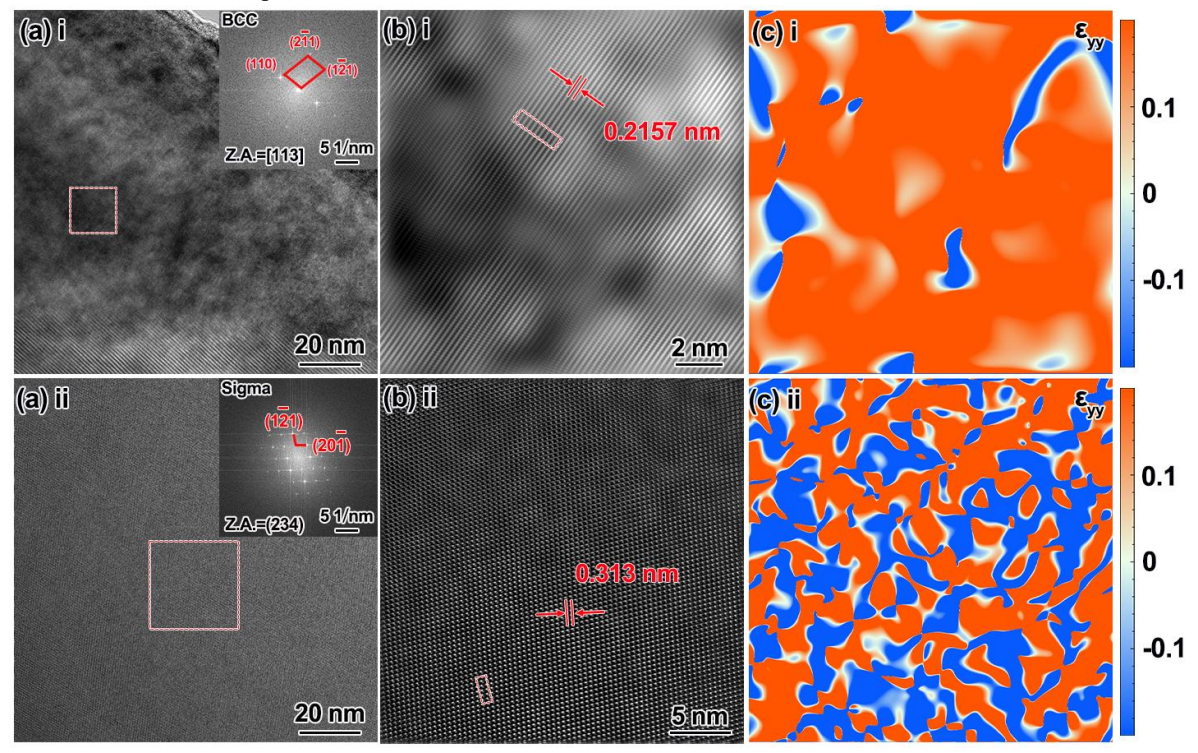


Fig. 6: TEM pattern of HT1050, where, (i) BCC, (ii) Sigma: (a) high-resolution spectrum, (b) IFFT, (c) stress field distribution

3.2 Mechanical property

Room temperature compression testing is an effective method for characterizing the mechanical properties of the materials. In this study, room temperature compression experiments of all alloys are conducted and the compressive stress-strain curves are shown in Fig. 7(a). The as-cast alloy exhibits a compressive yield strength of 570 MPa at room temperature and demonstrates good plasticity without fracture. After heat treatment at 1000 °C, the HT1000 alloy achieves a compressive yield strength of approximately 1040 MPa, with a compressive fracture strain of about 19.2%. Increasing the heat treatment temperature to 1050 °C, the alloy presents a compressive yield strength of approximately 1080 MPa and a fracture strain of about 21.2%. Further increasing the heat treatment temperature to 1100 °C leads to a compressive yield strength of about 872 MPa and a fracture strain of about 26.2% for the HT1100 sample. Notably, when the heat treatment temperature is raised to 1150 °C, the HT1150 alloy exhibits a compressive yield strength of 850 MPa, which is slightly lower than that of the HT1000, HT1050, and HT1100 alloys. However, the compressive fracture strain of the HT1150 alloy significantly increases to 34.6%, representing an improvement of about 63.2% compared

to the HT1050 alloy. When the heat treatment temperature is further increased to 1200 °C, the HT1200 alloy exhibits a compressive yield strength of approximately 650 MPa, which is 23.5% lower than that of the HT1150 alloy (850 MPa). Overall, the compressive yield strength of heat-treated alloys is higher than that of as-cast alloy at room temperature.

Microhardness testing is an effective method for characterizing the mechanical properties of materials. Fig. 7(b) presents the microhardness of all alloys. The microhardness of heat-treated alloys is consistently higher than that of as-cast alloy (351.7 HV). Specifically, as the heat treatment temperature rises from 1000 °C to 1050 °C, microhardness of the alloy increases. microhardness of HT1000 alloy is 514.1 HV and the microhardness of HT1050 alloy reaches 558.8 HV. However, further increasing the heat treatment temperature results in a decrease in microhardness. The HT1100 alloy shows a microhardness of 524.8 HV at 1100 °C heat treatment, and the microhardness drops to 372.7 HV after 1200 °C heat treatment. This indicates a negative correlation between microhardness and heat treatment temperature beyond 1050 °C. This is related to the change in the phase content of the hard and brittle Sigma phase in the alloy.

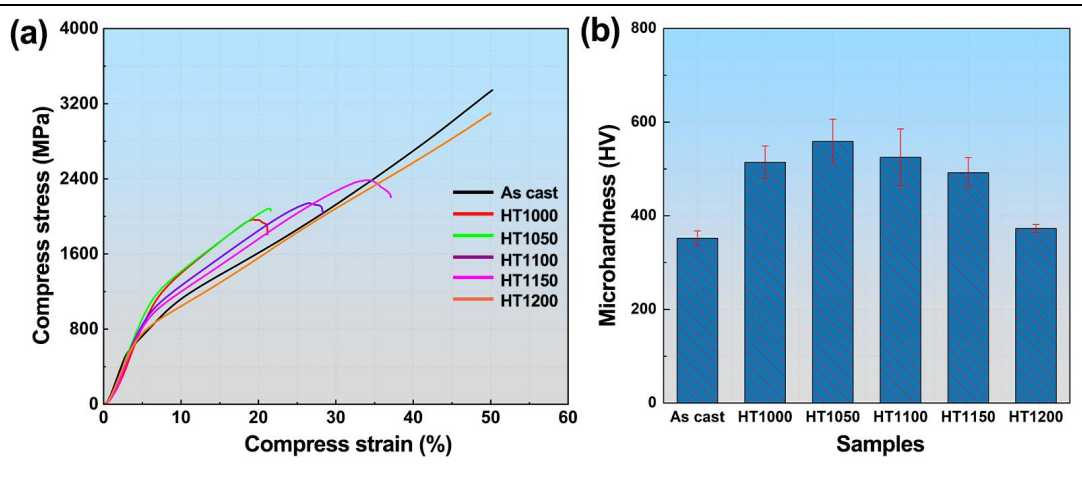


Fig. 7: Mechanical properties of all alloys: (a) compressive stress-strain curve at room temperature, (b) microhardness

The fracture mechanism of all alloys is explored in depth by SEM characterization of their compression fracture morphologies, as shown in Fig. 8. Notably, the as-cast and HT1200 alloys don't fracture during room-temperature compression. Fig. 8(a) reveals that the room-temperature compression fracture surface of HT1000 alloy exhibits significant brittle fracture characteristic, predominantly featuring relatively flat cleavage steps. When the heat treatment temperature increases to 1050°C, HT1050 alloy displays a

compression fracture morphology similar to HT1000 alloy, both showing brittle fracture (Fig. 8b). At 1100°C, the room-temperature compression fracture surface of HT1150 alloy shows numerous axial splitting features (Fig. 8c). Upon further heating to 1150°C, the axial splitting end of HT1150's fracture surface exhibits a hilly morphology with undulations (Fig. 8d), indicating its good room-temperature compression plasticity, which aligns with the room-temperature compressive stress-strain curve.

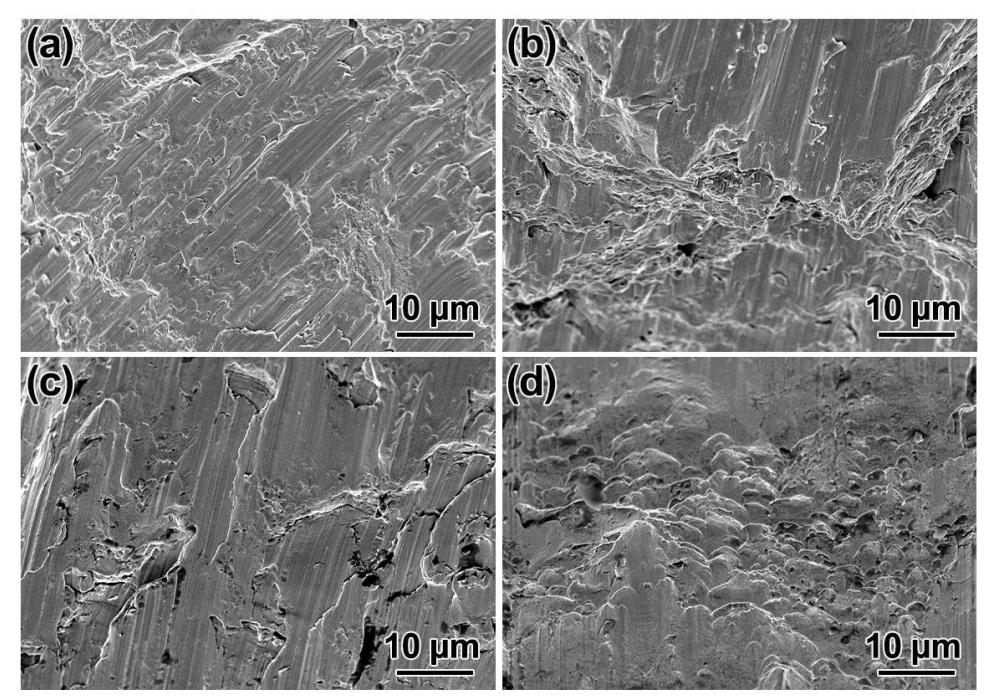


Fig. 8: Room-temperature compression fracture morphology of different alloys, (a) HT1000, (b) HT1050, (c) HT1100, (d) HT1150

4 Conclusions

In this study, the $Al_{0.4}CoCr_{0.6}NiV_{0.6}$ HEA alloy was heat-treated in the vacuum tube furnace. The phase content and distribution of the alloys were precisely controlled by adjusting the heat treatment temperature.

The influence of heat treatment temperature on the microstructure and mechanical properties of alloys was summarized, and the conclusions were as follows:

(1) The volume fractions of BCC and Sigma phases initially increased and then decreased with rising heat

treatment temperature. Under the heat treatment condition of 1050°C, the content of HT1050 alloy in the Sigma phase reached the maximum of 19.6%.

(2) Compared to the as-cast alloy, all alloys after heat treatment exhibited higher compressive yield strength. The compressive yield strength of HT1150 alloy reached

Acknowledgments

This work was supported by the National Natural Science Foundation of China (Grant No. 52175184, 52405213).

Conflicts of interest:

The authors declare that they have no known competing financial interests or personal relationships that could have appeared to influence the work reported in this paper.

References

- [1] Miracle D B. Senkov O N. A critical review of high entropy alloys and related concepts, Acta Mater. 2017, 122: 448-511.
- [2] Cui H B. Wang Y. Wang J Y. Guo X F. Fu H Z. Microstructural evolution and corrosion behavior of directionally solidified FeCoNiCrAl high entropy alloy, China Foundry. 2011, 3: 259-263.
- [3] He H. Wang Y. Qi Y. Xu Z. Li Y. Review on the preparation methods and strengthening mechanisms of medium-entropy alloys with CoCrNi as the main focus, J. Mater. Res. Technol. 2023, 27: 6275-6307.
- [4] Ramkumar K R. Park H. Lee J. Kwon H. Vikram R J. Kim E S. Zaragaran A. Kim H S. Development of a novel CoCrNi-based eutectic high entropy alloy for a wide temperature range, Mater. Sci. Eng. A. 2023, 885: 145606.
- [5] Li M Y. Qiu Y. Shi X. Liu Z Q. Birbilis N. Zhu Y M. Liu J. Nano-dispersion strengthened and twinning-mediated CoCrNi medium entropy alloy with excellent strength and ductility prepared by laser powder bed fusion, J. Alloys Compd. 2024, 1005: 176103.
- [6] Li Q X. Wang M L. Wang X D. Lu Y P. Wang T M. Partially recrystallized heterostructure via Mo-doping endows CoCrNi medium-entropy alloy with exceptional strength and ductility, Scripta Mater. 2024, 253: 116297.
- [7] Chang W C. Hsueh C H. Strengthening of CoCrNi medium entropy alloy with Ti additions, Intermetallics. 2023, 163: 108072.
- [8] Pan R C. Fan D. Bian Y L. Zhao X J. Zhang N B. Lu

- to 850 MPa, representing a 49.1% improvement over the as-cast alloy.
- (3) The microhardness of HT1050 alloy (351.7 HV) has increased by 58.9% compared with the as-cast alloy (558.8 HV). The strengthening effect mainly come from the hard and brittle phase Sigma in HT1050 alloy.
 - L. Cai Y. Luo S N. Effect of minor elements Al and Ti on dynamic deformation and fracture of CoCrNi-based medium-entropy alloys, Mater. Sci. Eng. A 2023, 884: 145535.
- [9] Yen J Y. Hsueh C H. Effects of Ti and Mo additions on microstructures and mechanical properties of CoCrNi medium entropy alloys, Mater. Sci. Eng. A 2025, 926: 147943.
- [10] Zheng X D. Chen H Y. Lu T W. Yao N. Wang Y G. Liu Y. Kosiba K. Laser additive manufacturing of CoCrNi medium entropy alloy composites reinforced by in-situ nanoprecipitations: Microstructure formation and mechanical properties, Mater. Charact. 2024, 207: 113500.
- [11] Luo S F. Wang N. Wang Y. Li X. Fang X G. Zhou H W. Chen J M. Yang X Y. Zhang J X. Achieving strength-ductility synergy of spark plasma sintered (CoCrNi)₉₄Al₃Ti₃ medium-entropy alloy via post-sintering in-situ precipitation treatment, J. Mater. Res. Technol. 2024, 33: 503-514.
- [12] Shahmir H. Asghari-Rad P. Mehranpour M S. Forghani F. Kim H S. Nili-Ahmadabadi M. Evidence of FCC to HCP and BCC-martensitic transformations in a CoCrFeNiMn high-entropy alloy by severe plastic deformation, Mater. Sci. Eng. A 2021, 807: 140875.
- [13] Saha J. Cobbinah P V. Hiroto T. Matsunaga S. Toda Y. Yamabe-Mitarai Y. Evolution of microstructure and texture in Al-containing CoCrNi medium entropy alloys during severe warm-rolling, Mater. Charact. 2024, 207: 113546.
- [14] Vashishtha H. Kumar D. Kim Y S. Lee S Y. Huang E W. Jain J. Effects of hot isostatic processing and hot rolling on direct energy deposited CoCrNi medium entropy alloy–Microstructural heterogeneity, wear behavior and corrosion characteristics, Mater. Charact. 2023, 205: 113304.
- [15] Luo J L. Lu H J. Wen M. Ma S G. Chen X Z. Exceptional strength-ductility synergy in additively manufactured (CoCrNi)₉₀Al₅Ti₅ medium-entropy alloy by heat treatment, J. Mater. Res. Technol. 2024, 31: 3642-3651.
- [16] Chang W C. Lu Y C. Hsueh C H. Oxide dispersion

- strengthening of CoCrNi medium entropy alloy using TiO₂ particles, Mater. Sci. Eng. A 2022, 859: 144196.
- [17] Chen X G. Qin G. Gao X F. Chen R R. Song Q. Cui H Z. Strengthening CoCrFeNi high-entropy alloy by Laves and boride phases, China Foundry. 2022, 19: 457-463.
- [18] Lu W J. Luo X. Wang Y F. Huang B. Wang Z J. Yang Y Q. γ" Phase transformation, precipitation hardening, hetero-deformation induced hardening and deformation mechanisms in a Nb-alloyed medium-entropy alloy, Mater. Des. 2023, 225: 111477.
- [19] Niu P D. Li R D. Fan Z Q. Cao P. Zheng D. Wang M B. Deng C. Yuan T C. Inhibiting cracking and improving strength for additive manufactured Al CoCrFeNi high entropy alloy via changing crystal structure from BCC-to-FCC, Addit. Manuf. 2023, 71: 103584.
- [20] Zhang X C. Wan B. Ding L P. Wang C L. Lei X C. Weng Y Y. Jia Z H. Effect of Al and Nb addition on the precipitation hardening and deformation mechanism of CoCrNi medium entropy alloy, J. Alloys Compd. 2024, 992: 174619.
- [21] Shi Y Z. Li B. Hou X H. Li C. Wu D. Gao Y M. Bai P C. Liu Y. Liang C Y. Microstructure and mechanical properties of CoCrNiVAl_x multi-principal component alloy, J. Mater. Res. Technol. 2024, 31: 3515-3525.
- [22] Wu D. Li B. Shi Y Z. Hou X H. Li C. Gao Y M. Bai P C. Liu Y. Liang C Y. Effects of different Al contents

- on mechanical properties and high temperature oxidation resistance of AlxCoCr0.6NiV0.6 high entropy alloy, J. Alloys Compd. 2025, 1025: 180348.
- [23] Uporov S A. Ryltsev R E. Bykov V A. Estemirova S K. Zamyatin D A. Microstructure, phase formation and physical properties of AlCoCrFeNiMn high-entropy alloy, J. Alloys Compd. 2020, 820: 153228.
- [24] Huang L R. Fu Z Q. Chu C L. Chen W P. Wang H. Zhu D Z. Microstructure and mechanical behavior in a spherical L1₂ nanoprecipitates strengthened Ni₃₅Co_{27.5}Cr_{27.5}Al₅Ti₅ high-entropy alloy fabricated by direct casting and heat treatment, J. Alloys Compd. 2024, 1002: 175299.
- [25] Ji Z Y. Qiu C L. Achieving superior high-temperature strength in an additively manufactured high-entropy alloy by controlled heat treatment, Appl. Mater. Today. 2024, 40: 102412.
- [26] Peng H L. Hu L. Huang S M. Baker I. Effects of heat treatment on the microstructure and mechanical properties of a nanoparticle-strengthened medium-entropy alloy produced by electron-beam powder bed fusion, J. Alloys Compd. 2025, 1021: 179598.
- [27] Sun Y G. Zhang C J. Ning Z L. Sun J F. W Ngan A H. Huang Y J. Additively manufactured low-gradient interfacial heterostructured medium-entropy alloy multilayers with superior strength and ductility synergy, Compos. B Eng. 2024, 280: 111522.